

## CHAPTER 2

## EXPERIMENTAL SET-UP AND DATA ANALYSIS

### 2.1. Experimental set-up:

In the present investigation the air shower array operating at the North Bengal University (NBU) ( atmospheric depth  $\sim 1000\text{g cm}^{-2}$  , latitude  $26^{\circ}45'N$  , longitude  $88^{\circ}21'$  ) is designed to detect electrons and muons of various energies simultaneously. The array is sensitive to air showers initiated by cosmic ray primaries of energy in the range  $10^{14}$ - $10^{16}$  eV.

#### 2.1.1. NBU air shower array:

The NBU EAS array for observation of air showers has been developed in stages since 1980 (Basak et al [1] ). At present the air shower array has nineteen plastic scintillation detectors for the measurement of electron density , eight fast timing detectors to determine the arrival directions of the detected EAS and two magnet spectrographs ( maximum detectable momentum  $500\text{ GeV}/c$  , each of area  $1\text{m} \times 1\text{m}$  and cut off at an energy  $2.5\text{ GeV}$  ) with a spacing of  $4\text{m}$  to measure the momentum of muons in EAS. The lay-out of the detectors shown in fig.2.1 covers an area of about  $1200\text{ m}^2$  with detector spacing of about  $8\text{m}$ .

#### 2.1.2 Electron density detectors:

Scintillation detectors are used in the NBU air shower experiment to detect the EAS particles. Plastic scintillators each of size  $50\text{cm} \times 50\text{cm}$  and width  $5\text{ cm}$  are kept within a pyramidal light tight aluminium enclosure. The inner surfaces of the enclosure are coated with a highly reflecting material composed of titanium dioxide ( $\text{TiO}_2$ ). A Dumont 6364 photomultiplier tube separated by a distance of about  $39\text{ cm}$  from the plastic scintillator is placed to view the scintillations produced in the scintillator . Performance of each detector was studied by measuring the single particle pulse height. To measure the single particle pulse height, each scintillation counter is placed along a line of alignment of G.M counter telescope as shown in fig.2.2. Out of three G.M. counters one is crossed and the scintillation counter is placed in such a way that if a charged particle passes through the four counters it

120547  
25 MAR 1998

~~CONFIDENTIAL~~  
University Library  
North Bengal University

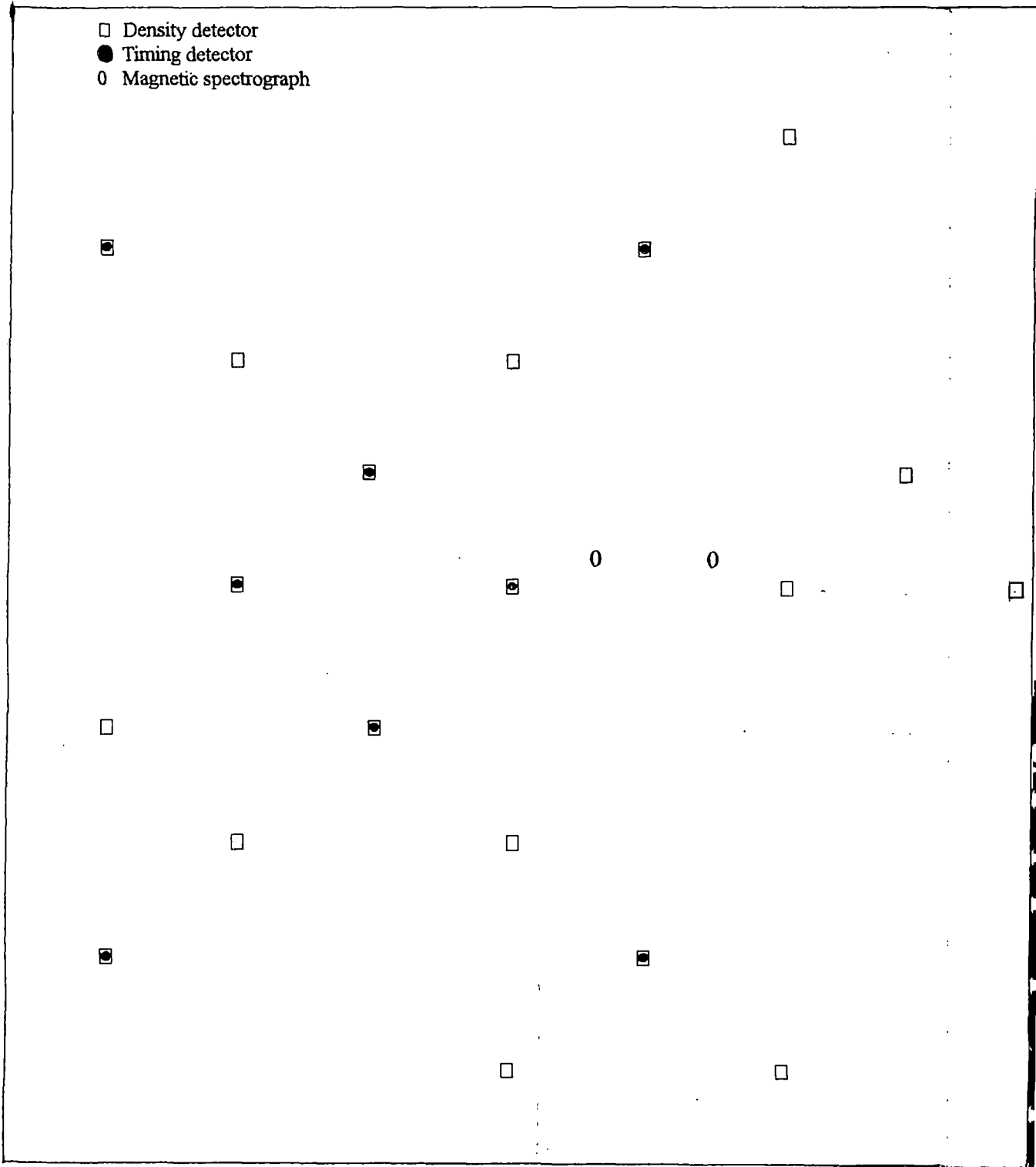


Fig. 2.1. The NBU EAS array

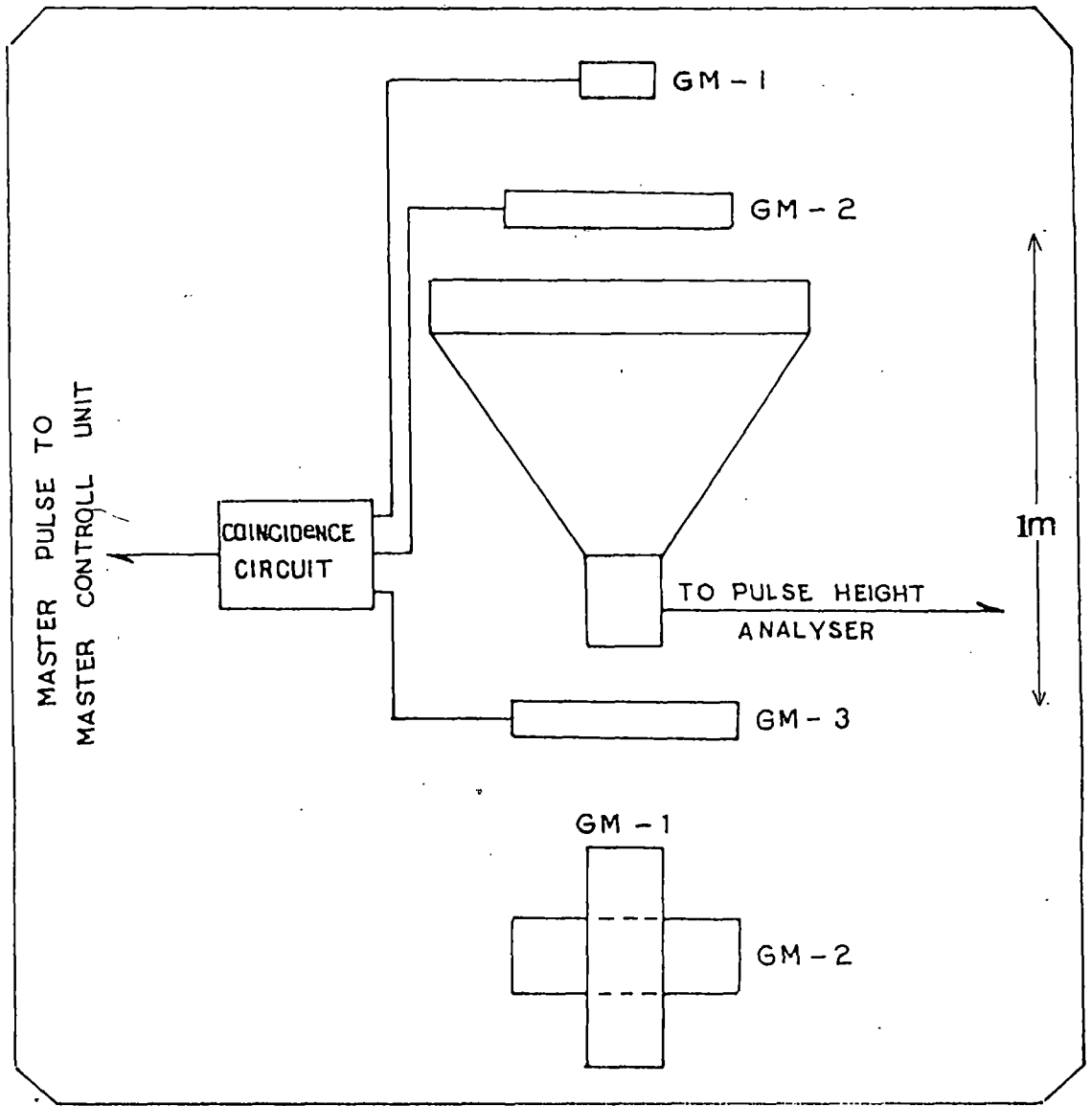


Fig. 2-2. Arrangement for measuring single particle pulse height .

produces four negative pulses at the output of the four counters. The three G.M. pulses are used for the coincidence. For the measurement of pulse height the coincidence pulse from the three G.M. counters is used to trigger the Master Control Unit and the output from the plastic scintillator is connected to the first channel of the pulse height measuring circuit. The digitised output represents the scintillation counter pulse height. The experiment is repeated for all the detectors and different voltages in the range 850-1200 Volts are applied to different photomultiplier tubes to ensure that the single particle pulse height in different detectors are nearly same. The relative efficiency in terms of single particle pulse height is nearly uniform from centre to edge of each plastic scintillation detector.

### **2.1.3. Fast timing detectors:**

Eight fast timing detectors are employed in the NBU air shower experiment to measure relative time delays between their output pulses to determine the arrival direction of a detected EAS. The shape and size of the scintillator and enclosure of these detectors are the same as the electron density detectors but Philips fast photomultiplier tubes (XP 2020, rise time 1.5 ns) are used in stead of relatively slow photomultipliers (rise time ~ 20-30 ns) used in the electron density detectors.

### **2.1.4. Magnetic spectrograph unit:**

Two identical magnet spectrograph units separated by a distance of 4m are operated under an EAS trigger to detect the muons of EAS particles. The arrangement of the magnetic spectrograph unit is shown in fig.2.3. Each magnet spectrograph consists of a solid iron magnet in between four neon flash tube trays. The solid iron magnet is composed of 80 low carbon content steel plates (180 cm x 125 cm x 1.25 cm) having a rectangular hole (35 cm x 19 cm) at the centre. Both the longer arms of the magnets are wound with 600 turns of double cotton covered copper wire. The power requirement for each magnet when operated at 15 amp. current is 2.3 kilowatts. There are four neon flash tube trays ( $T_1, T_2, T_3, T_4$ ), two of which are placed above the magnet and other two are placed below the magnet for the accurate location of muon trajectory as shown in fig.2.3. Each neon flash tube tray consists of 120 neon flash tubes arranged in 8 layers and each layer contains 15 tubes. The tubes in each tray are staggered in such a way that a single particle

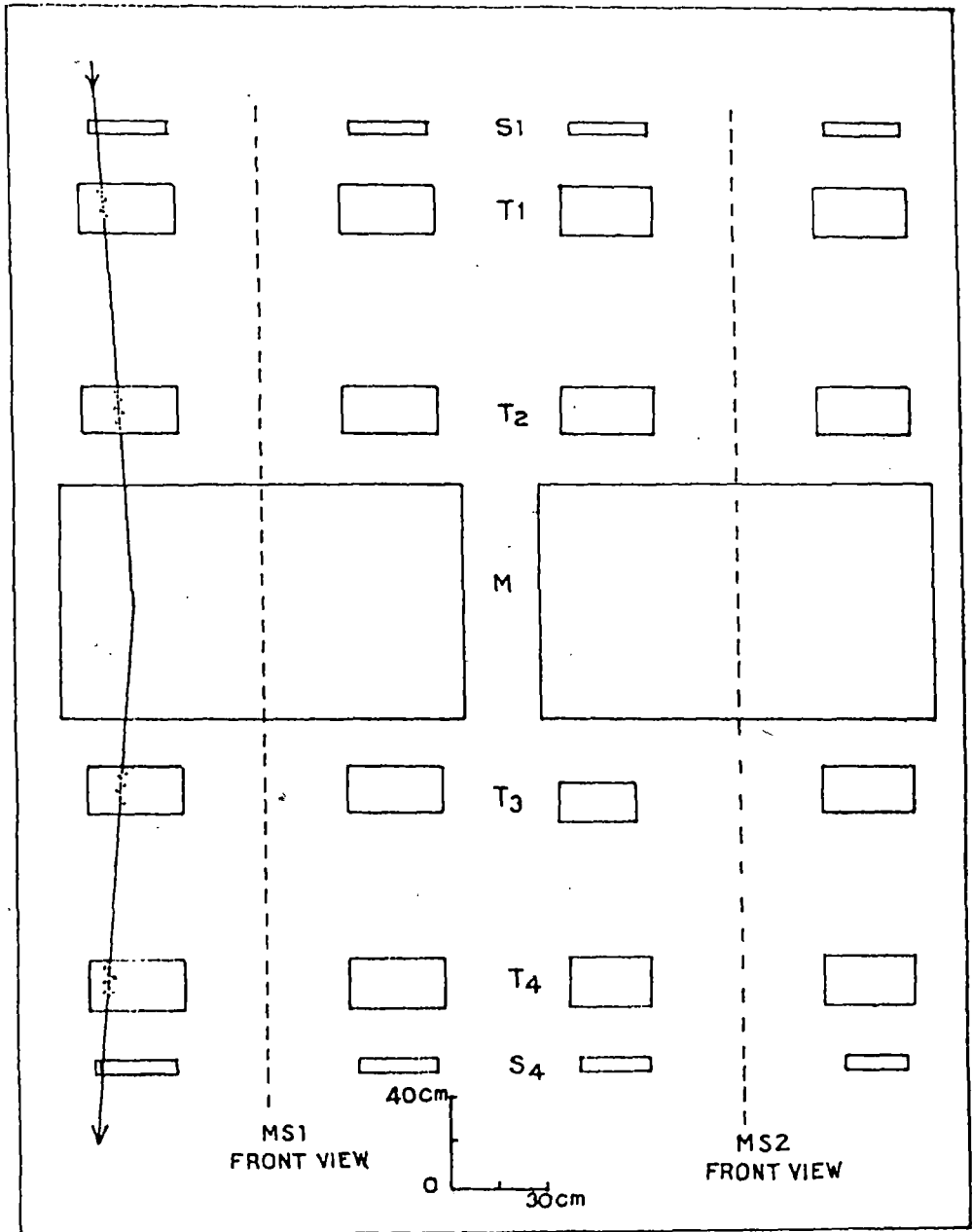


Fig. 2-3. Schematic diagram of magnetic spectrograph unit .

passing through a tray must traverse at least four tubes . The arrangement of the flash tubes in a tray is shown in fig.2.4. The tubes in each tray are supported by duraluminium bars by means of milling machine at Central Mechanical Research Institute , Durgapur,India. Thin aluminium electrodes are placed in between two layers of neon flash tubes. The horizontal separation between two tubes is  $1.999 \pm 0.002$  cm which is referred to as one tube separation ( t.s ) unit. The vertical separation between two tubes of adjacent layers is 2.8 cm . Four cameras are used to record the flashes of the neon flash tubes photographically. To remove the electronic components an absorber of concrete of about 1m-thick is used at a distance of about 1m above the spectrograph unit on the roof of the laboratory building . Moreover, lead absorber of about 5cm thick is also placed above the top tray of the spectrograph to absorb any electron component .

#### **2.1.5. Principle of operation of the NBU EAS array:**

The data acquisition system in the NBU EAS set-up can be divided into four parts - shower selection system (coincidence circuit) , timing data handling system , density data handling system and muon data handling system . The actual circuit diagram and detailed discussion of the control electronics of the whole data acquisition system are given in [2]. Here only the operation of different parts of the data acquisition system are discussed briefly in the following section. The block diagram of the data acquisition system is shown in fig.2.5.

#### **2.1.6. Shower selection system:**

Shower is recorded by the shower selection system if the registered electron density in any four adjacent detectors of the eight central triggering detectors is greater than 4 particles/m<sup>2</sup>.

#### **2.1.7. Timing data handling system:**

The output pulses from eight fast timing plastic scintillation detectors are fed to the discriminator (Lecroy 623B) and level adopter ( Lecroy 688 AL) unit with equal time delay by means of equal length RG 58 cables. The shower event is selected by means of a four fold fast coincidence within 50 ns time delay. This four

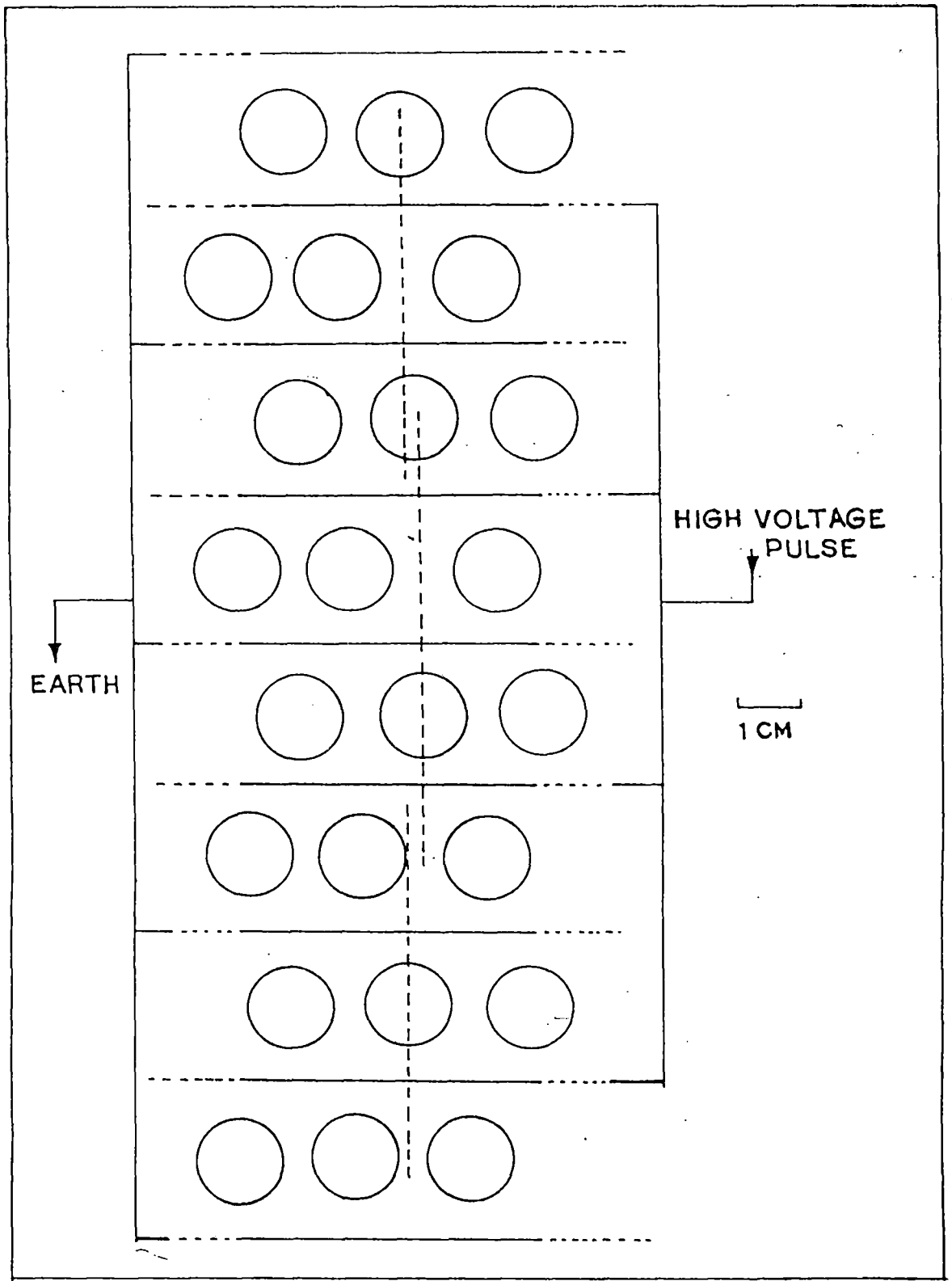


Fig. 2-4. The staggering arrangement of the flash-tubes in a tray of magnetic spectrograph units .



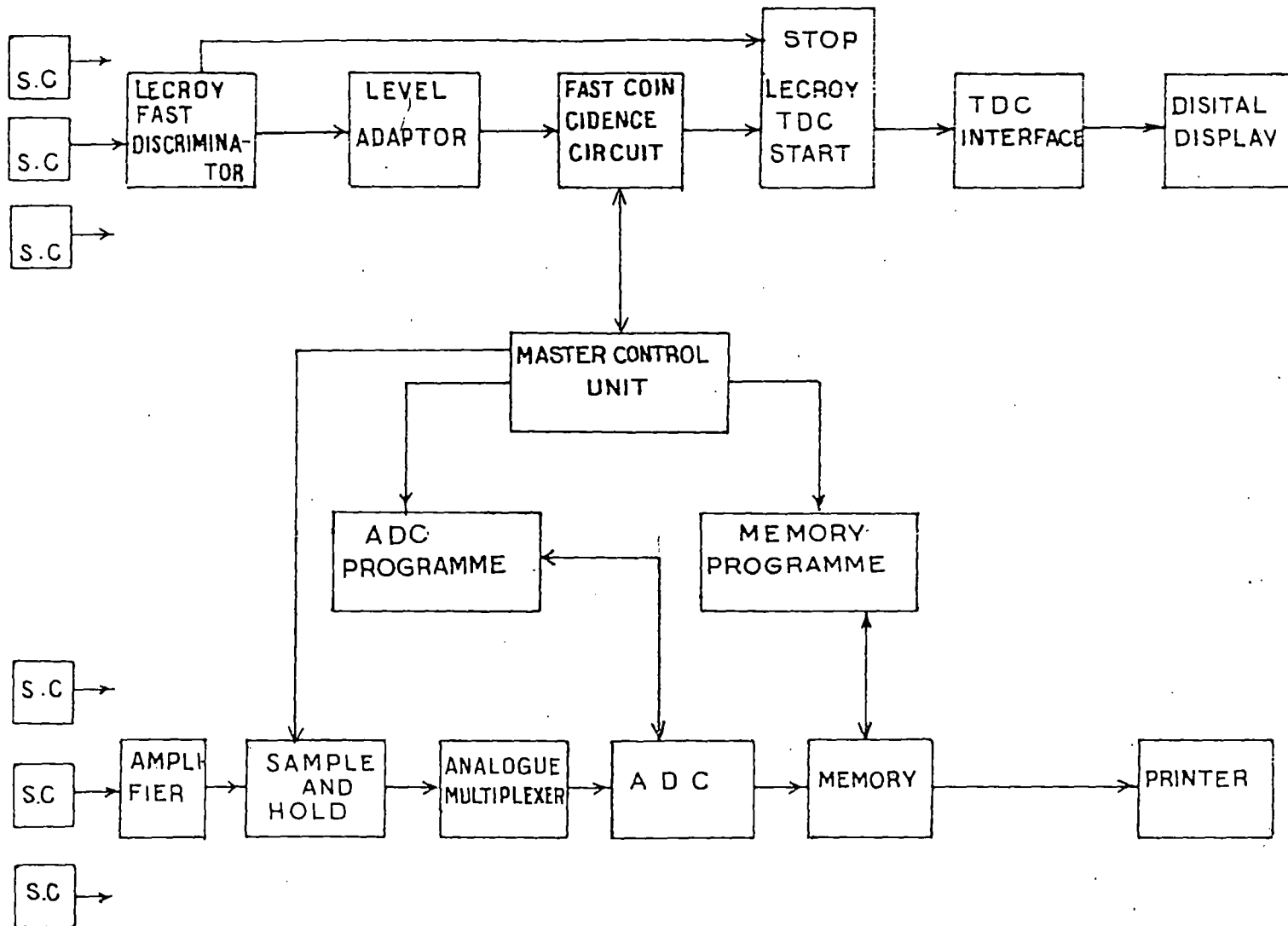


Fig. 2.5. Block diagram of the data handling system.

fold coincidence pulse ( start pulse ) is used to start the TDC system (Lecroy 2228A) and the Master Control unit (MCU) of the density recording system . At the same time this four fold coincidence pulse is used for the input Veto of the four fold coincidence circuit. The common start pulse of the input of TDC unit starts charging the capacitors of eight channels and are stopped by the relative arrival of eight pulses (stop pulse) from fast timing detectors through 172ft RG 174 cables for equal amount of delay. The different amount of charge stored in eight channels correspond to the relative arrival times of eight pulses from fast timing scintillation detectors. These charges are converted directly to times by the method of discharge and their corresponding digitized forms are stored in the memory of TDC unit. At the end of storing the data into the memory a manual switch is used by which the digitized data are displayed. Then the Veto is withdrawn for the next event.

#### **2.1.8. Density data handling system:**

The analogue outputs from nineteen scintillation detectors of the array after amplification first by preamplifiers and then by main amplifiers are fed to the Sample and Hold circuit by charging capacitors for about  $3\mu\text{s}$  after the triggering of the MCU unit by a master pulse generated from a four fold coincidence . At the end of  $3\mu\text{s}$  , these capacitors will discharge and will be ready to accept the next input pulses. As soon as the MCU unit is triggered , it gives a hold command to the Sample and Hold circuit , switches off the input lines by an analogue switch and disconnects the coincidence circuit from MCU unit and sends a start pulse to the ADC (analogue to digital converter[3] ) programme unit. Once ADC programme unit is triggered , it connects all the pulses at the output of the Sample and Hold [4] circuit by the analogue multiplexer one after the other to the ADC . The total time to scan the nineteen channels is about 8 msec. After scanning the first channel the ADC gives a write pulse to the memory for writing the digital information in the memory . As soon as the counting in the first channel is over , the ADC programme unit initiates the multiplexer to connect the second channel and write the digital information to the memory in the similar way . After completion of scanning for all the channels , a read pulse is generated from the memory programme unit which in turn operates on the memory unit for recording the digital information on a paper tape by a line printer. After this operation (33 sec) the analogue switch is opened and it switches on the input lines for the next event .

### **2.1.9. Muon data handling system:**

Each spectrograph unit is placed in between two scintillation detectors to select the vertical muons passing through it. When muon passes through the spectrograph, a two fold coincidence pulse is generated and if this pulse occurs in coincidence with the air shower then it is fed to the base of a power transistor. The output pulse from the power transistor fires a thyatron (5C22/XH-16-200) which in turn discharges a condenser ( 0.05  $\mu\text{f}$  ) charged to 12kV through a 100 ohm non-inductive resistance . The resulting high voltage pulse is then applied to the electrode plates between the flash tube layers. The rise time and the time delay between the passage of the particle through the spectrograph and the application of the pulse to the flash tube trays are 0.75 $\mu\text{s}$  and 5 $\mu\text{s}$  respectively . In the presence of the high voltage , the gas in the neon flash tubes ionize and glow when muon passes through the tubes . Four cameras are used to record the muon trajectories from the flashes of the neon tubes.

## **2.2. Data analysis:**

The present experiment has been continued from January 1994 to September 1995 and in the mean time 16,000 shower data associated with 2927 muon data have been collected . The shower data have analysed by Fortran language in a 486-DX2 computer and the momentum of muons have measured by means of projector method . Artificial shower analysis has been carried out to obtain the errors in the measurement of shower parameters.

### **2.2.1. Shower data analysis:**

The output (P) printed on the paper tape for a particular detector is related to the electron density  $\Delta$  as given by

$$\Delta = P / (A \cdot H)$$

where A is the area of the detector and H is a constant representing the mean of the single charged particle pulse height distribution.

The measured charged particle densities in individual EAS are fitted to a fitting function to determine the parameters ( $N_e$ ,  $X_0$ ,  $Y_0$ ,  $s$ ) of the detected shower. The fitting function by Hillas et al [5] as given below is chosen in the present analysis.

$$\Delta(r) = (N_e/r_0^2) \cdot c(s) \cdot [ (r/r_0)^{a1+a2(s-1)} (1+r/r_0)^{b1+b2(s-1)} ] \text{----- (2.1)}$$

where  $c(s)$  is the normalisation constant and the parameters are chosen for best fit of the experimental results as  $r_0=24\text{m}$ ,  $a1= -0.53$ ,  $a2= 1.54$ ,  $b1= -3.39$ ,  $b2= 0$ .

### **2.2.2. Determination of shower parameters:**

The estimation of the shower parameters namely the shower size ( $N_e$ ), shower core ( $X_0$ ,  $Y_0$ ) and shower age ( $s$ ) are necessary for the complete description of a shower. The shower size gives the total number of shower particles present in the shower at the level of observation. The shower core is a point in the shower plane having maximum shower particle density and the shower age parameter describes the longitudinal development of the shower. Even though the density of particles measured is due to all charged particles yet the measured densities can be approximated to electron densities without appreciable error since the density of the non-electronic components present in a shower is almost a few percent of that of the electrons.

The shower parameters are determined by fitting Hillas function to the observed electron densities at different points by minimising the quantity

$$\chi^2 = \sum_i W_i (\Delta_i^o - \Delta_i^e)^2 \text{----- (2.2)}$$

with respect to all the shower parameters simultaneously. Here  $\Delta_i^o$  is the observed particle density in the  $i$ th detector,  $\Delta_i^e$  is the expected particle density in the same detector which is calculated by substituting the estimated shower parameters in the Hillas function. The weight factor  $W_i$  is taken as

$$W_i = 1/ \Delta_i^e{}^2$$

The summation is over all the detectors which record the densities. The condition of minimisation of  $\chi^2$  with respect to the shower parameters is given by

$$\delta\chi^2/\delta Q_i = 0 \quad ; \quad i = 1 \text{ to } 4 \text{----- (2.3)}$$

where  $Q_i$  are the four shower parameters ( $N_e$ ,  $s$ ,  $X_0$ ,  $Y_0$ ). The above equations are highly non-linear and difficult to solve analytically. So independent estimation of the shower parameters are not possible from the above equations. Hence an iterative procedure is necessary to estimate the shower parameters. In the present analysis the steepest descent iterative process by using the gradient search method of minimizing  $\chi^2$  is taken.

Initially  $\chi^2$  is set at a large value and  $s$  is taken as 1.2. The initial estimation of the core location ( $X_0$ ,  $Y_0$ ) is made by using the following two equations

$$X_0 = \frac{\sum_i \Delta_i^0 \cdot X_i}{\sum_i \Delta_i^0}$$

$$Y_0 = \frac{\sum_i \Delta_i^0 \cdot Y_i}{\sum_i \Delta_i^0}$$

where  $X_i$ ,  $Y_i$  are the co-ordinates of the  $i$ th detector. With these values of  $X_0, Y_0$  the initial estimation of the shower size ( $N_e$ ) is made by solving the equation

$$\delta\chi^2 / \delta N_e = 0 \quad \text{----- (2.4)}$$

which yields a cubic equation of the form

$$N_e^3 + a.N_e + b = 0 \quad \text{----- (2.5)}$$

where  $a$  and  $b$  are functions of the core location and age.

From these values of  $X_0, Y_0, s$  and  $N_e$ , the quantity  $\chi^2$  and its gradient  $\nabla\chi^2$  for various components are evaluated. If the new value of  $\chi^2$  is less than its initial value, the parameters are then changed in accordance to the respective components of  $\nabla\chi^2$  and a new set of parameters are obtained. The process is continued until the difference between the two successive values of  $\chi^2$  per degree of freedom is less than 0.001. When this condition is reached the present value of the shower parameters are taken as the best fitted values. If it is found that within 500 iterations the above condition is not reached, then the current values of

the parameters are taken because in such cases it has been found that the value of  $\chi^2$  oscillate very close to the minimum value . A flow chart to measure the shower parameters is shown in fig.2.6.

Three forms of fitting function  $f(r/r_0,s)$  have been taken and tested the goodness of fit to the observed density distribution of particles in EAS in a previous experiment of different EAS array lay-out by Bhattacharyya et al [6] . These are : NKG function  $f_{\text{NKG}}(r/r_0,s)$  [7] , Hillas function  $f_{\text{H}}(r/r_0,s)$  [5] and Capdevielle function  $f_{\text{C}}(r/r_0,s)$  [8] . The forms of these three functions ( $f_{\text{NKG}}$  ,  $f_{\text{H}}$  ,  $f_{\text{C}}$ ) are given in chapter 1. The observed probability distribution  $P_\chi$  corresponding to  $\nu$  degrees of freedom for the reduced  $\chi_\nu^2 (= \chi^2/\nu)$  for a given shower size over the whole radial range 0-120m using NKG , Hillas and Capdevielle functions are shown in figs.2.7,2.8 and 2.9 . The mean values of the reduced  $\chi_\nu^2$  for the three distribution functions are given in table 2.1 and it is seen that  $f_{\text{H}}(r/r_0,s)$  among the three distributions is the best fit to the observed distribution in the radial range 0-120m.

Table 2.1. Mean values of the reduced  $\chi_\nu^2$  from figs.2.7,2.8 and 2.9 for the distribution functions (for EAS radial range 0-120m)

$f_{\text{NKG}}(r/r_0,s)$	$f_{\text{H}}(r/r_0,s)$	$f_{\text{C}}(r/r_0,s)$
1.81	1.77	1.80

An examples of observed shower data and reconstructed shower parameters from the observed data for an EAS events is shown in fig.2.10. Chi-square distribution for experimentally observed shower data and artificial shower data are shown in fig.2.11 .

### 2.2.3. Muon data analysis :

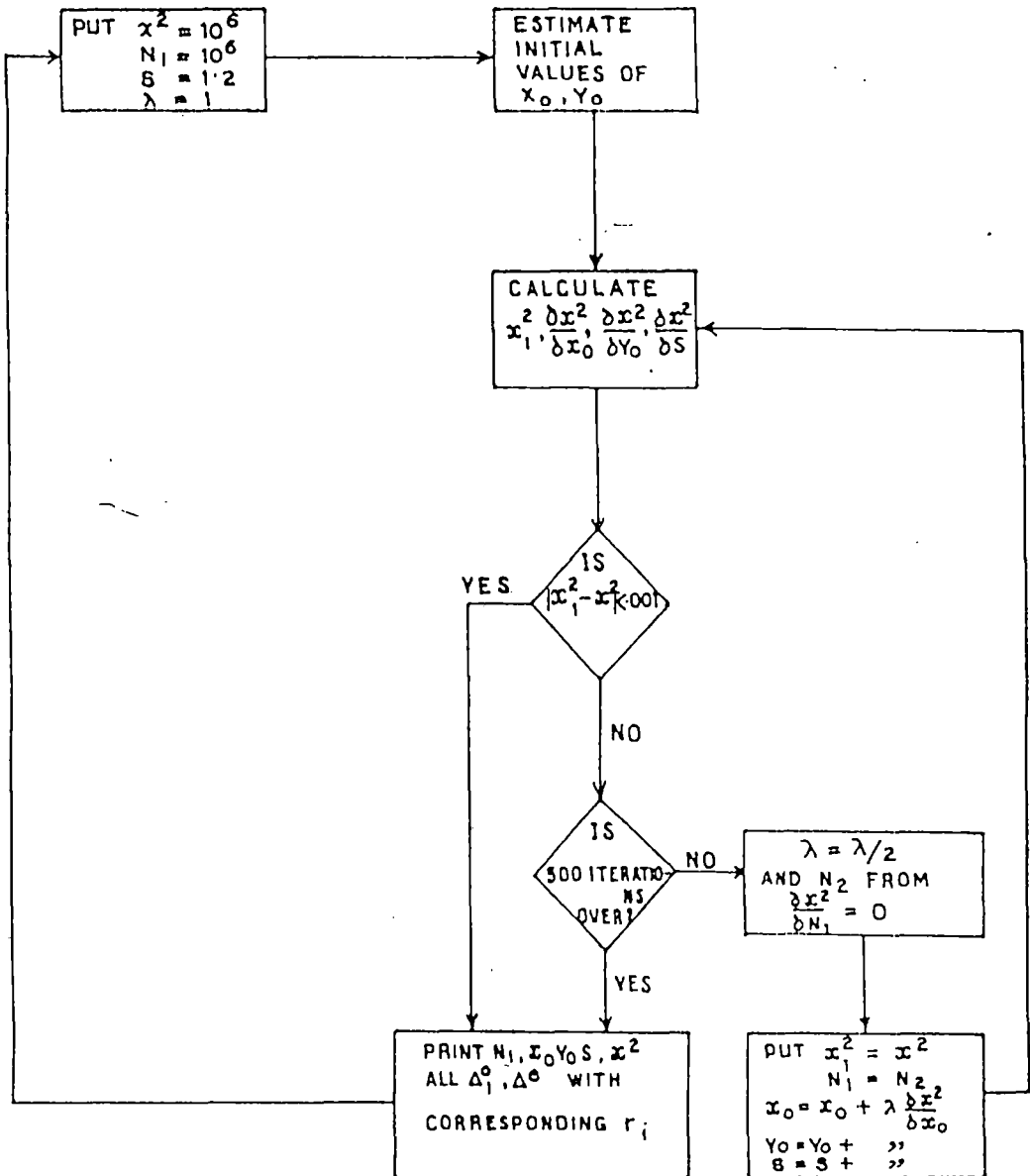


Fig. 2.6. Flow chart for  $x^2$ -minimisation.

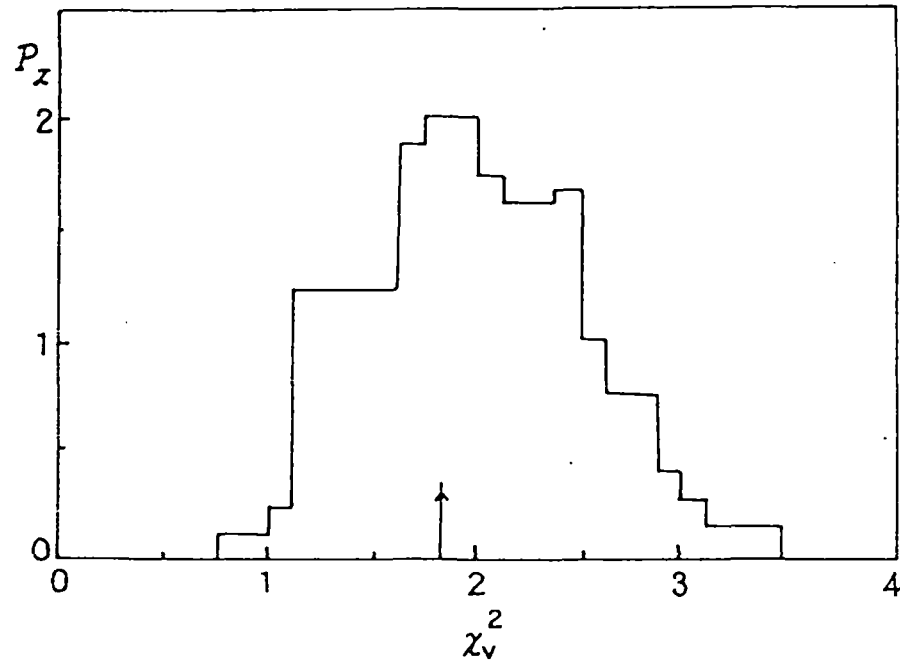


Fig. 2.7. The observed probability distribution  $P_z$  for the reduced chi square  $\chi_v^2$  using the NKG function in the radial range 0-120m.



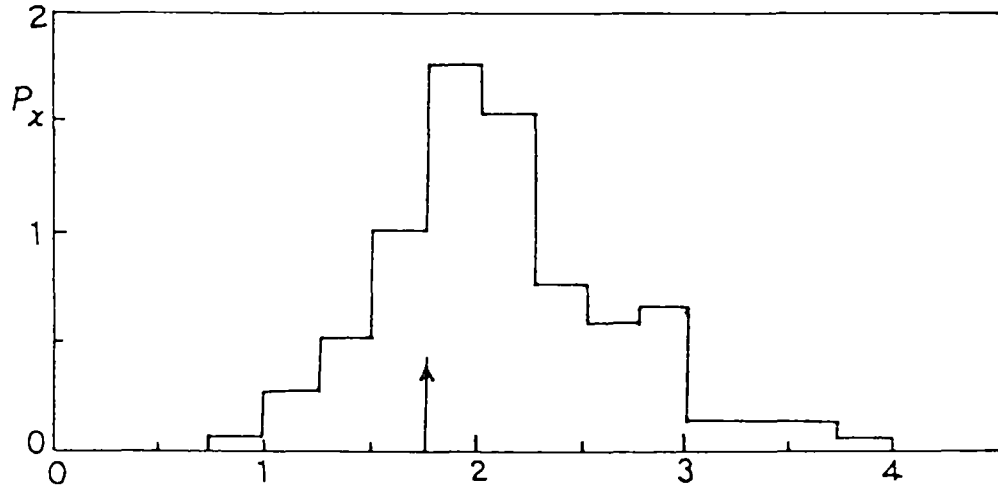


Fig. 2.8: The observed probability distribution  $P_x$  for the reduced chi square  $\chi^2_y$  using the Hillas function in radial range 0-120 m.

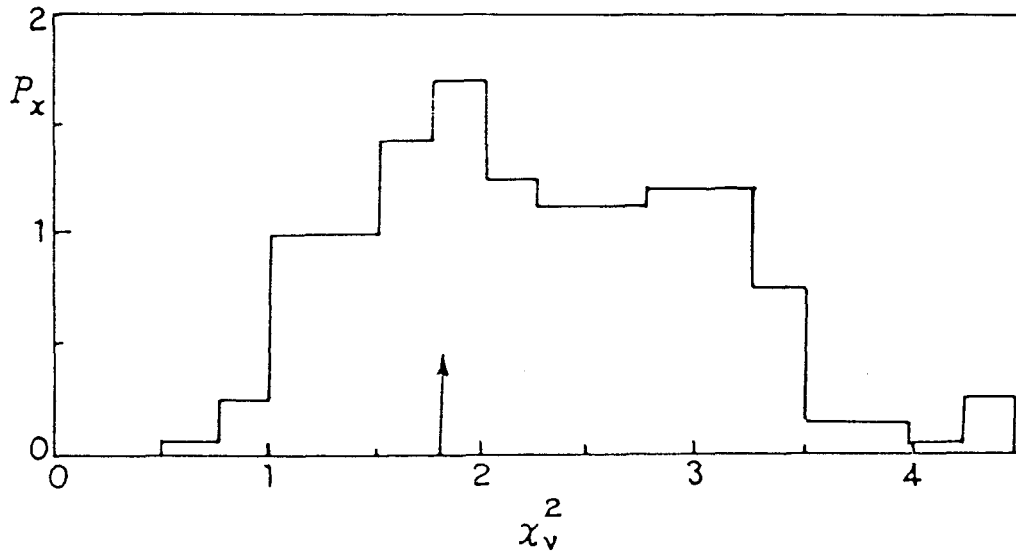


Fig.2.9. The observed probability distribution  $P_x$  for the reduced chi square  $\chi_v^2$  using the Capdevielle function in the radial range 0-120 m.

Event number : 2669

Date:12.2.94

Chi-square (per degree of freedom) : 0.582

Shower core :  $X_0 = 29.19\text{m}$  Shower size ( $N_e$ ) =  $6.2 \times 10^4$

$Y_0 = 20.99\text{m}$  Shower age (s) = 1.13

Distance (r) in m.	Fitted density in particles/m <sup>2</sup>	Observed density in particles/m <sup>2</sup>
7.65	26.12	22.93
22.40	5.00	6.04
22.75	4.85	2.67
15.35	9.93	10.52
9.59	19.75	17.42
17.65	7.79	7.47
15.23	10.03	8.71
12.84	13.16	17.60
8.73	22.25	18.67
21.27	5.54	4.44
14.60	10.77	10.24

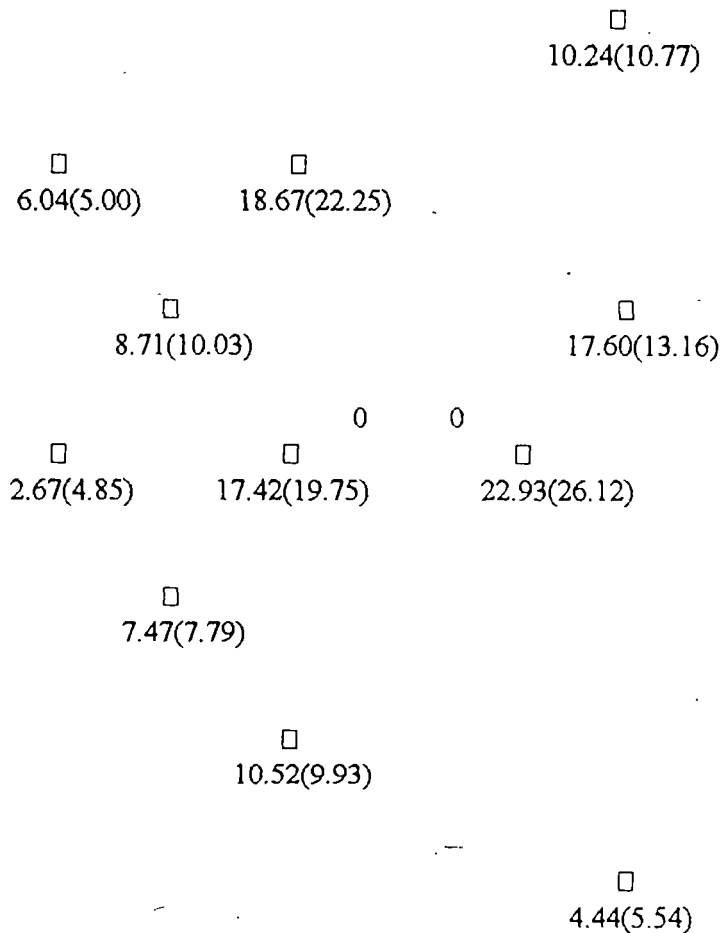


Fig.2.10. Observed shower data and reconstructed shower parameters from the observed data

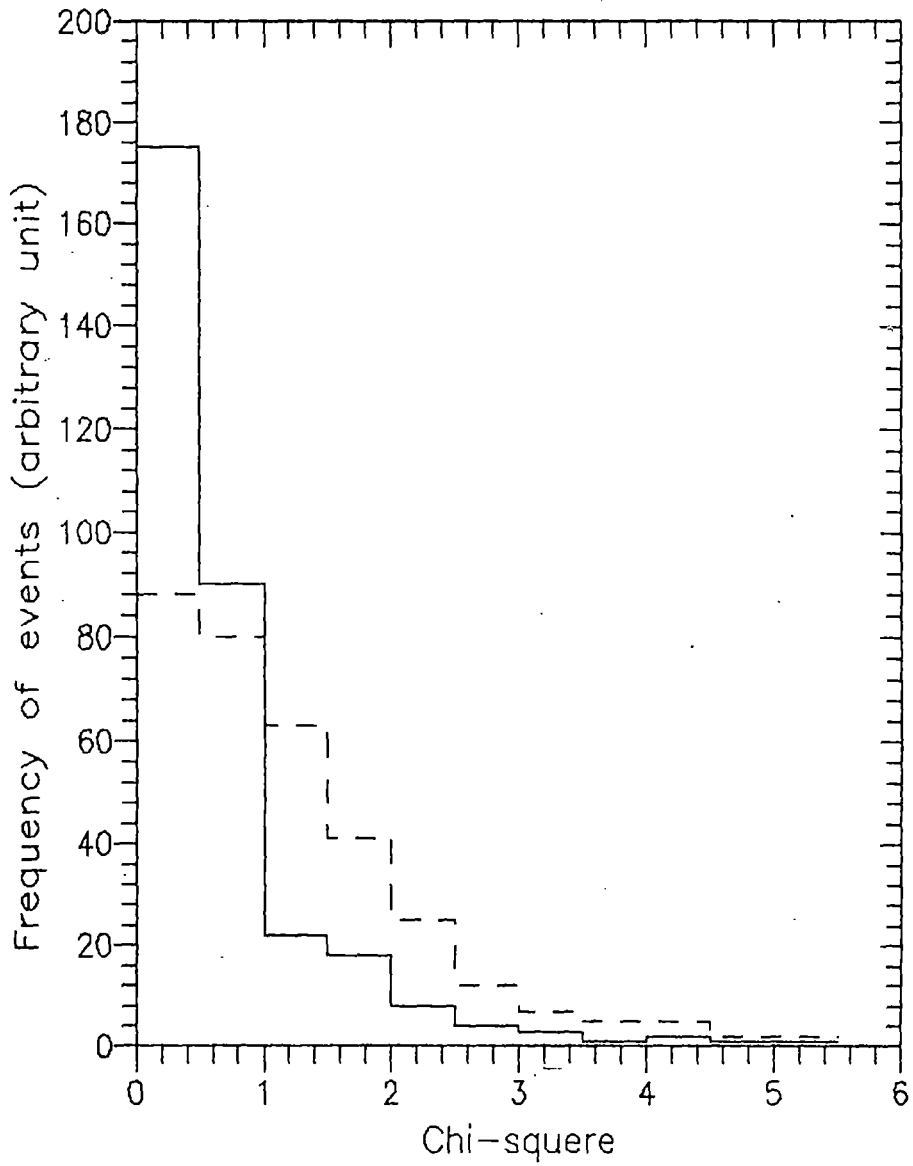


Fig.2.11. Chi-square distributions for experimentally observed shower data(dashed line)and for artificial shower data (solid line)

The momentum of a muon is measured from the deflection of its path in the magnetic field . A particle of momentum  $P$  and charge  $e$  moving transversely through a magnetic field of induction  $B$  is related to the radius of curvature  $R$  of its path given by

$$P = 300.B.R \text{ (eV/c)} \quad \text{-----} \quad (2.6)$$

where  $B$  is in Gauss ,  $R$  is in cm.

If  $dl$  be the length of the element of path traversed by the particle normal to the field and  $d\phi$  be the deflection of the particle due to magnetic field , then

$$R = dl/d\phi \quad \text{-----} \quad (2.7)$$

Neglecting energy loss in the material of the magnet , the momentum of the particle can be written as

$$P = (300 \text{ B}dl) / \phi \quad \text{-----} \quad (2.8)$$

where  $l$  is in cm. ,  $\phi$  is in radian and  $P$  is in eV/c.

A schematic diagram of the magnetic spectrograph along with the particle trajectory is shown in fig.2.12. The deflection in the magnetic field is calculated from the four measured co-ordinates along the length of the trajectory .  $FT_1, FT_2, FT_3, FT_4$  are four neon flash tube trays which determine the particle trajectory. The reference line  $ACEG$  is at a distance  $a_0, b_0, c_0, d_0$  from the four flash tube trays respectively.  $CL$  is the central line of the spectrograph and the effective length of the magnet is  $2L$  where  $2L = 106.3$  cm.  $X_1, X_2$  are the distances of the trays as shown in fig.2.12 where  $X_1=31.85$  cm.,  $X_2 = 85$  cm.,  $L+X_1=X_2=85$  cm.

Since  $\phi$  is the deflection at the central place of the magnet  $M$  ,

$$FT_1.FT_2 = FT_3.FT_4$$

If a perpendicular line is drawn from  $H'$  on  $EF'$  , we get from the geometry of the particle trajectory ,

$$GH' - EF' = CD - AB \quad \text{.....} \quad (2.8a)$$

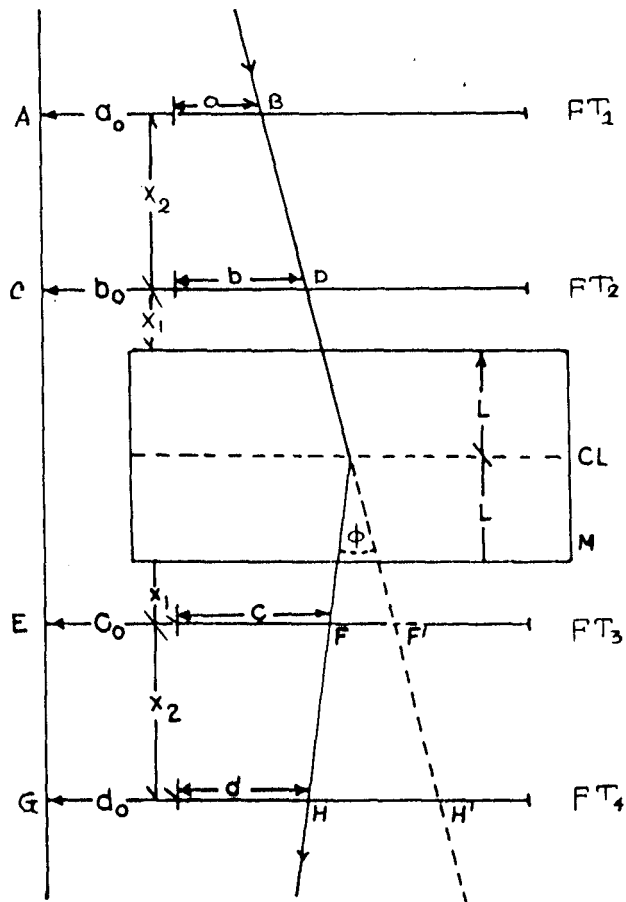


Fig. 2.12 A schematic diagram of the magnetic spectrograph along with the particle trajectory.

$$\text{or, } (GH + HH') - (EF + FF') = CD - AB$$

$$\text{Now, } HH' = \phi(L + X_1 + X_2), FF' = \phi(L + X_1)$$

$$\text{Hence, } GH' = GH + HH' = (d_0 + d) + \phi(L + X_1 + X_2)$$

$$EF' = (c_0 + c) + \phi(L + X_1)$$

Using equation 2.8a, we get,

$$(d_0 + d) + \phi(L + X_1 + X_2) - (c_0 + c) - \phi(L + X_1) = (b_0 + b) - (a_0 + a)$$

$$\text{or, } \phi X_2 + (d + d_0) - (c + c_0) = (b + b_0) - (a + a_0)$$

$$\text{or, } \phi = [\{(b + b_0) - (a + a_0)\} + \{(c + c_0) - (d + d_0)\}] / X_2$$

Now we can write

$$\begin{aligned} \phi &= (\Delta_0 + \Delta_m) / X_2 \\ &= \Delta / X_2 \end{aligned} \quad \text{-----(2.9)}$$

$$\text{where } \Delta_0 = (b_0 - a_0) + (c_0 - d_0)$$

$$\text{and } \Delta_m = (b - a) + (c - d)$$

The quantity  $\Delta_0$  is the geometrical constant of the magnetic spectrograph and  $\Delta_m$  is the geometrical constant due to magnetic deflection.

From equations 2.8 and 2.9, we have

$$\begin{aligned} P &= 300 \text{ Bdl}/\phi \\ &= 300 \cdot B \cdot 2L \cdot X_2 / \Delta \\ &= C / \Delta \quad (\text{eV}/c) \end{aligned}$$

$$\text{where } C = 300 \cdot B \cdot 2L \cdot X_2$$

For the NBU magnetic spectrograph,  $B = 1.62 \times 10^4$  Gauss,  $2L = 106.3$  cm.,  $X_2 = 85$  cm.

$$\text{Hence } C = 300 \times 1.62 \times 10^4 \times 106.3 \times 85 / 1.999 \quad (\text{eV}/c)(\text{t.s})$$

$$\text{and } P = 21.96 / \Delta \quad (\text{GeV}/c) \quad \text{----- (2.10)}$$

where  $\Delta$  is in t.s unit (1 t.s = 1.999 cm.)

The momentum can be calculated from equation 2.10 by measuring the quantity  $\Delta$ . The values of  $a_0$ ,  $b_0$ ,  $c_0$ ,  $d_0$  are measured from the alignment of the spectrograph and  $a$ ,  $b$ ,  $c$ ,  $d$  are measured by using the projector method as discussed below.

To obtain the exact position of the tubes flashed in the trays, first, the films are projected on the vertical board by a 35 mm film projector. All the boards contain the serial number of the tubes with respect to the fiducial marks. With the aid of the fiducial marks, images of the flashed tubes are positioned on this reference board and the row number and the column number for each tray are recorded on a data sheet. Hence after determination of  $a$ ,  $b$ ,  $c$ ,  $d$  for each muon event equation 2.10 is used for the calculation of momentum of a muon passing through the magnetic spectrograph.

#### **2.2.4. Error estimation in the measured shower parameters:**

To have any confidence in the experimental results, it is essential to have an idea of the errors in the value of the shower parameters determined by the minimisation procedure discussed in sec.2.2.2 since all the properties of EAS are defined in terms of the shower parameters. The errors arise owing to fitting a fluctuated set of densities to an average lateral distribution function and also owing to the arbitrary criteria for locating the minimum of the  $\chi^2$ -surface. If the  $\chi^2$ -surface is flat, we may be far away from the minimum even though the criteria for the minimum is satisfied. An artificial shower analysis is done for this purpose.

The errors in the determination of shower parameters have been evaluated by using the standard procedure of artificial shower analysis. A shower of known parameters is allowed to be incident at any point within the array selected at random and the particle density in each detector is calculated according to the Hillas function [5]. To reproduce the experimental conditions, the statistical fluctuations in the number of particles in each detector and the systematic error in the conversion of pulse height into particle density are superposed on each detector. For a set of densities for each shower,  $\chi^2$ -minimisation procedure is applied to estimate the shower parameters. The estimated shower parameters deviate from the corresponding shower parameters used for an artificial shower and the deviations are given below



- (1)  $\Delta X = \pm 2.4 \text{ m}$
- (2)  $\Delta Y = \pm 2.7 \text{ m}$
- (3)  $\Delta N_e/N_e = \pm 9.6\%$
- (4)  $\Delta s = \pm 0.13$

Some histograms for the deviations of the parameters are shown in figs. 2.13, 2.14, 2.15 and 2.16.

### 2.2.5. Sensitivity of the EAS array:

Showers of all sizes with their cores at all points are recorded so long as they satisfy the triggering condition as discussed in sec. 2.1.6 but the detection efficiency and triggering probability for a particular shower size are dependent on the distance from the centre of the array. Therefore to observe the sensitivity of the EAS array, the detection efficiency and triggering probability at different  $N_e$  and  $s$  have to be determined.

#### **Detection efficiency of the EAS array:**

The efficiency of detection is nothing but the fraction of showers that were selected. To find the detection efficiency  $\epsilon(N_e, s, X, Y)$  at any point  $(X, Y)$  of the array for detecting showers of size  $N_e$  and age  $s$ , the circular symmetry of the array was used because of reduced numerical computation. The array was divided into a number of annular rings. Showers with fixed size  $N_e$  and  $s$  were uniformly selected in an annular ring and the expected density at each detector was calculated by using Hillas function. To these densities, the Poissonian and systematic errors were superposed. Then the selection criteria was applied and checked whether the particular shower was selected or not. A total of 1000 showers were generated in each annular ring. The computation was repeated by varying the shower size  $N_e$  and distance bin. The variation of detection efficiency with radial distance for different  $N_e$  and  $s$  are shown in figs. 2.17, 2.18, 2.19 and 2.20. If  $R_0$  is the distance from the centre of the array at which the detection efficiency is 90%, the 90% efficient area of the array is  $\pi R_0^2$ .

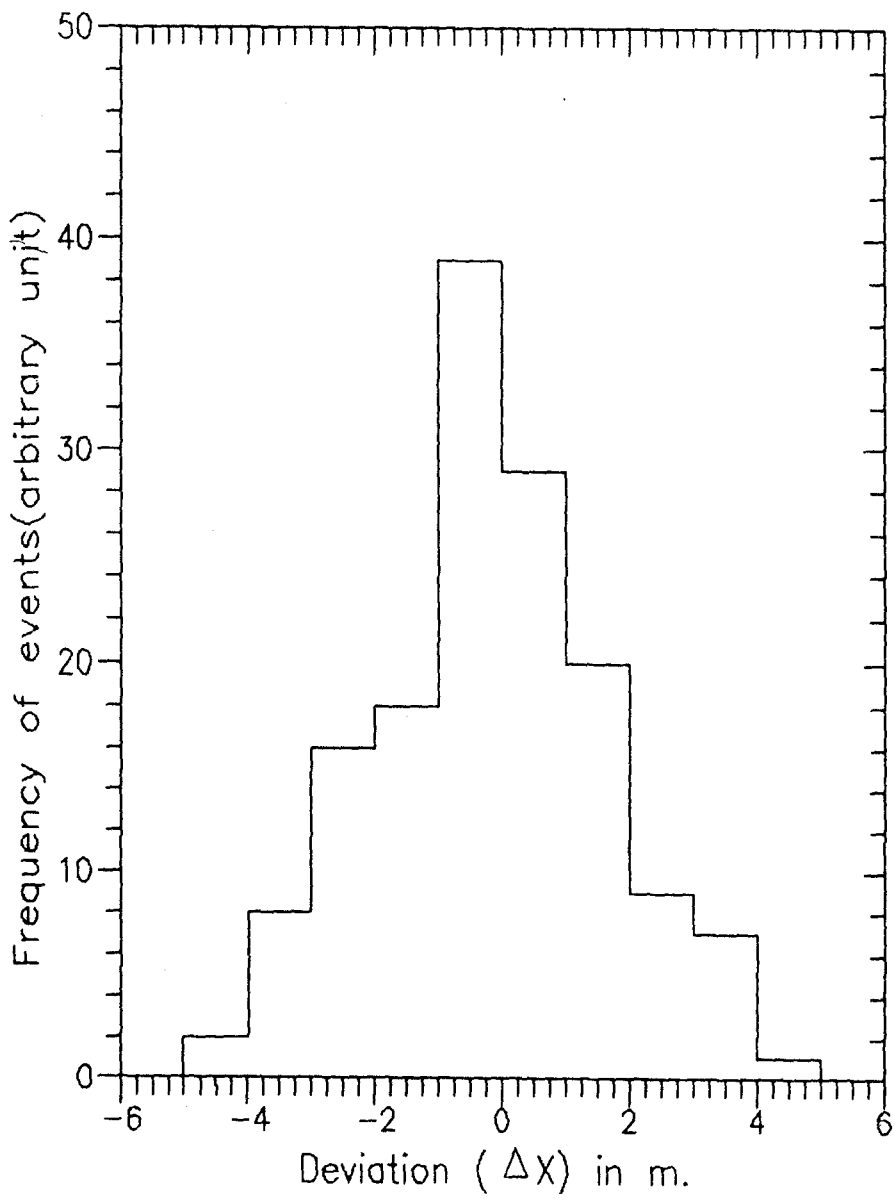


Fig.2.13. Frequency distribution of deviations in core location along the X-axis

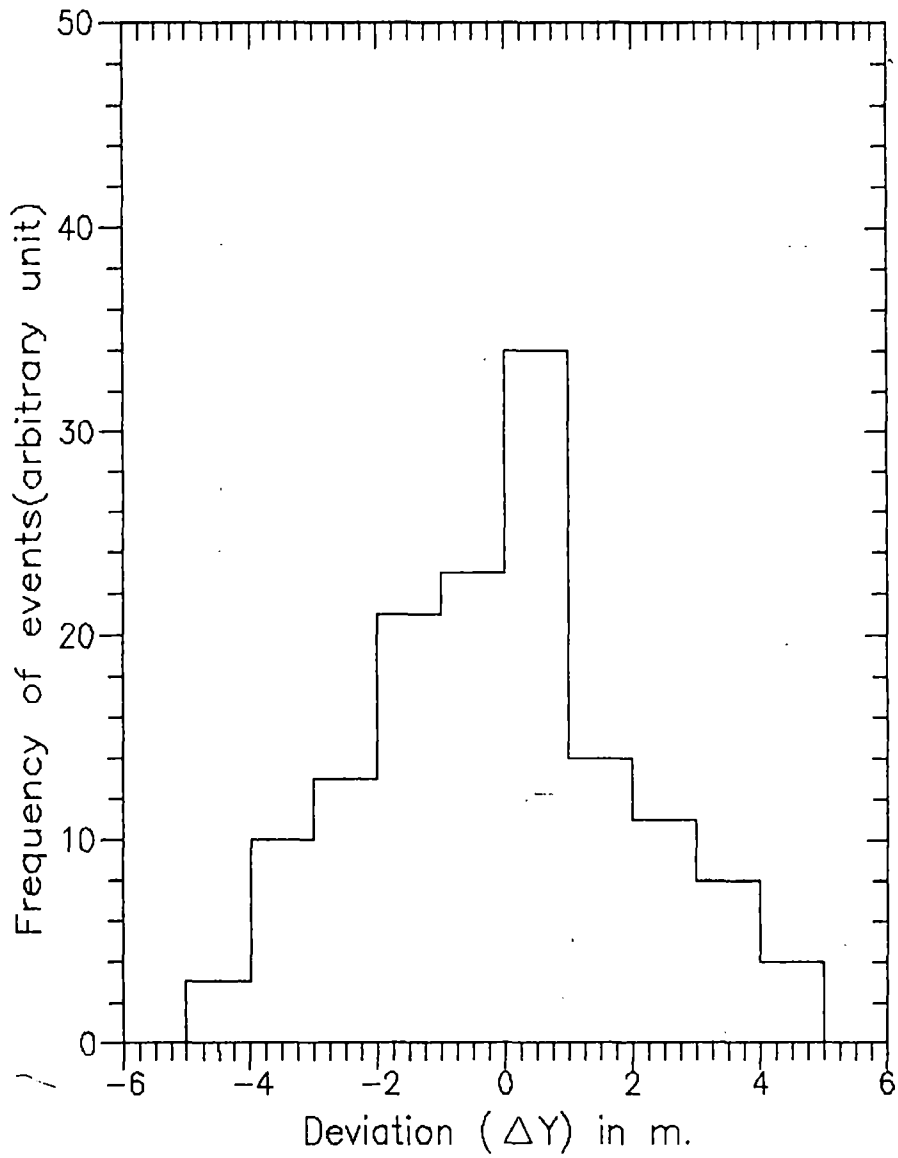


Fig.2.14. Frequency distribution of deviations in core location along the Y-axis

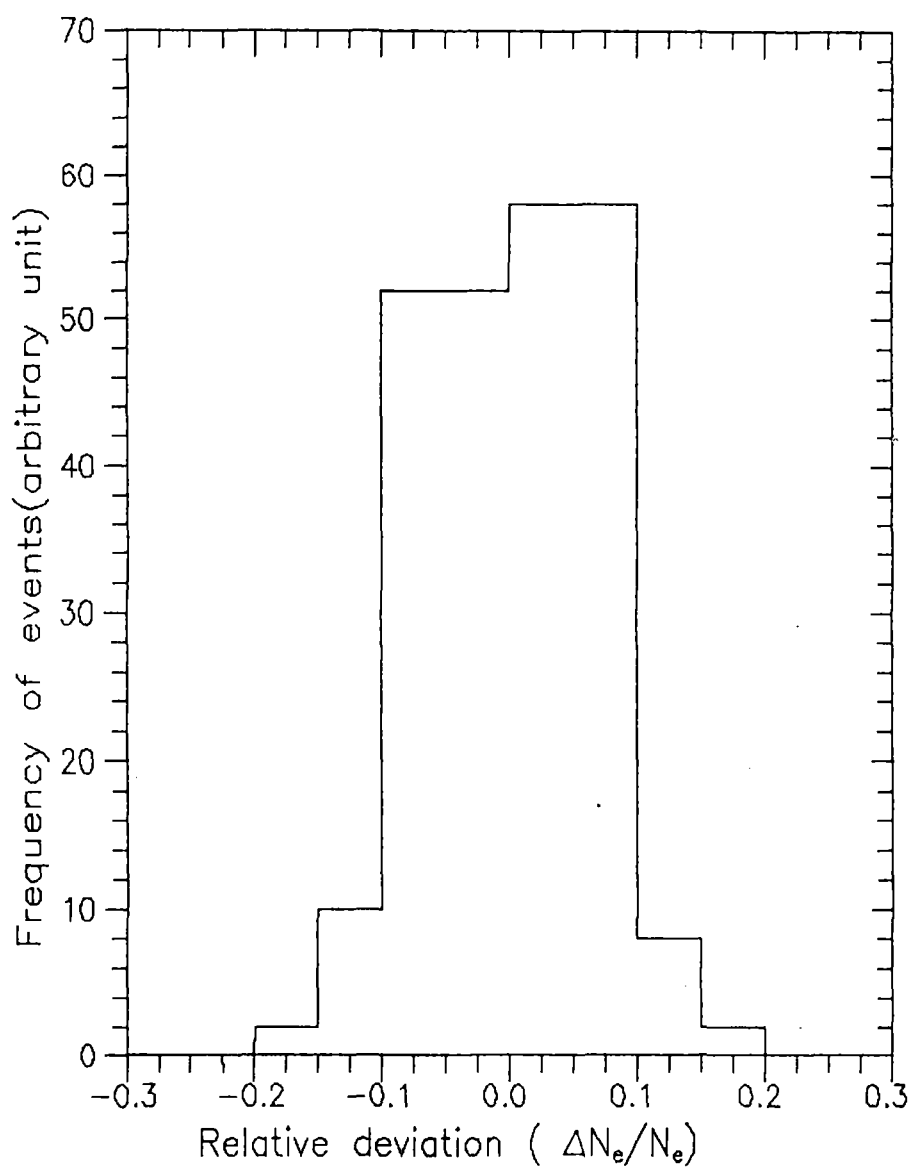


Fig.2.15. Frequency distribution of deviations in shower size

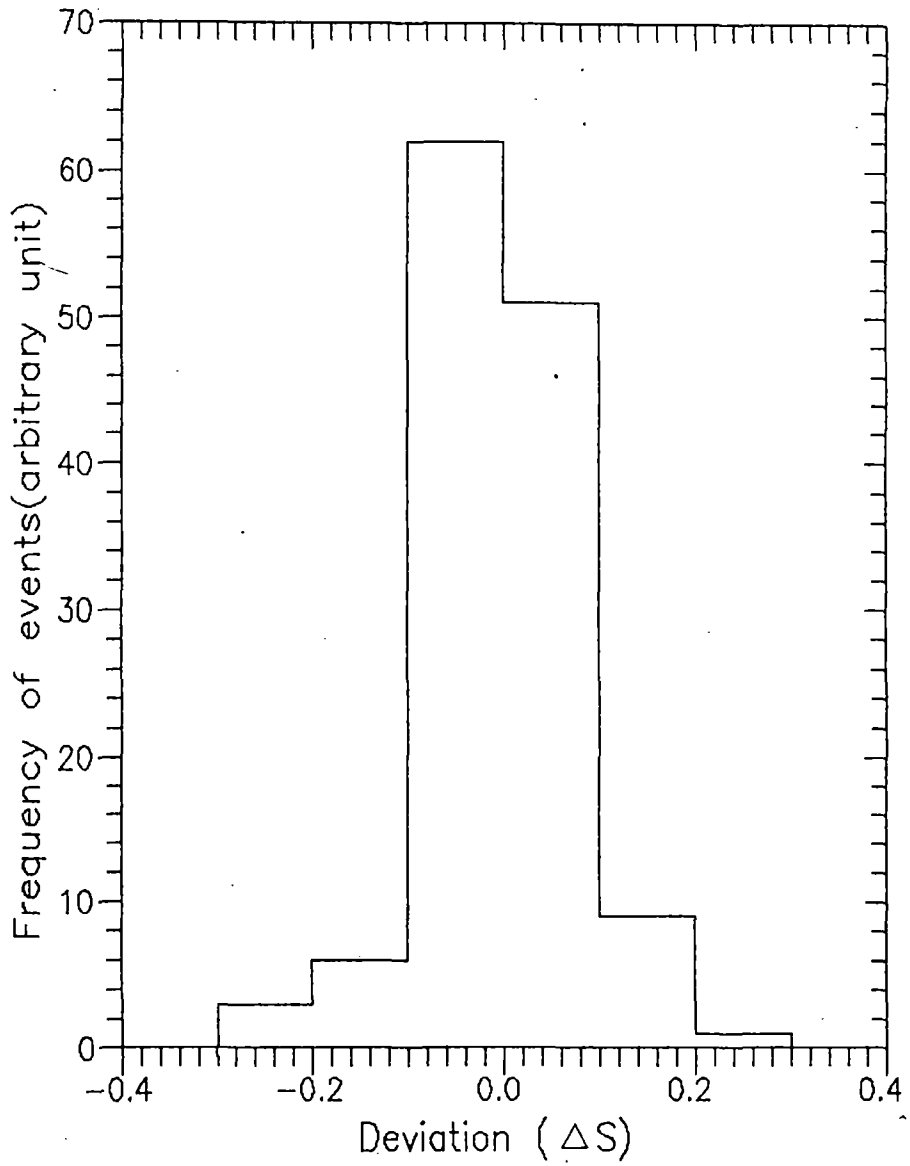


Fig.2.16. Frequency distribution of deviations in shower age

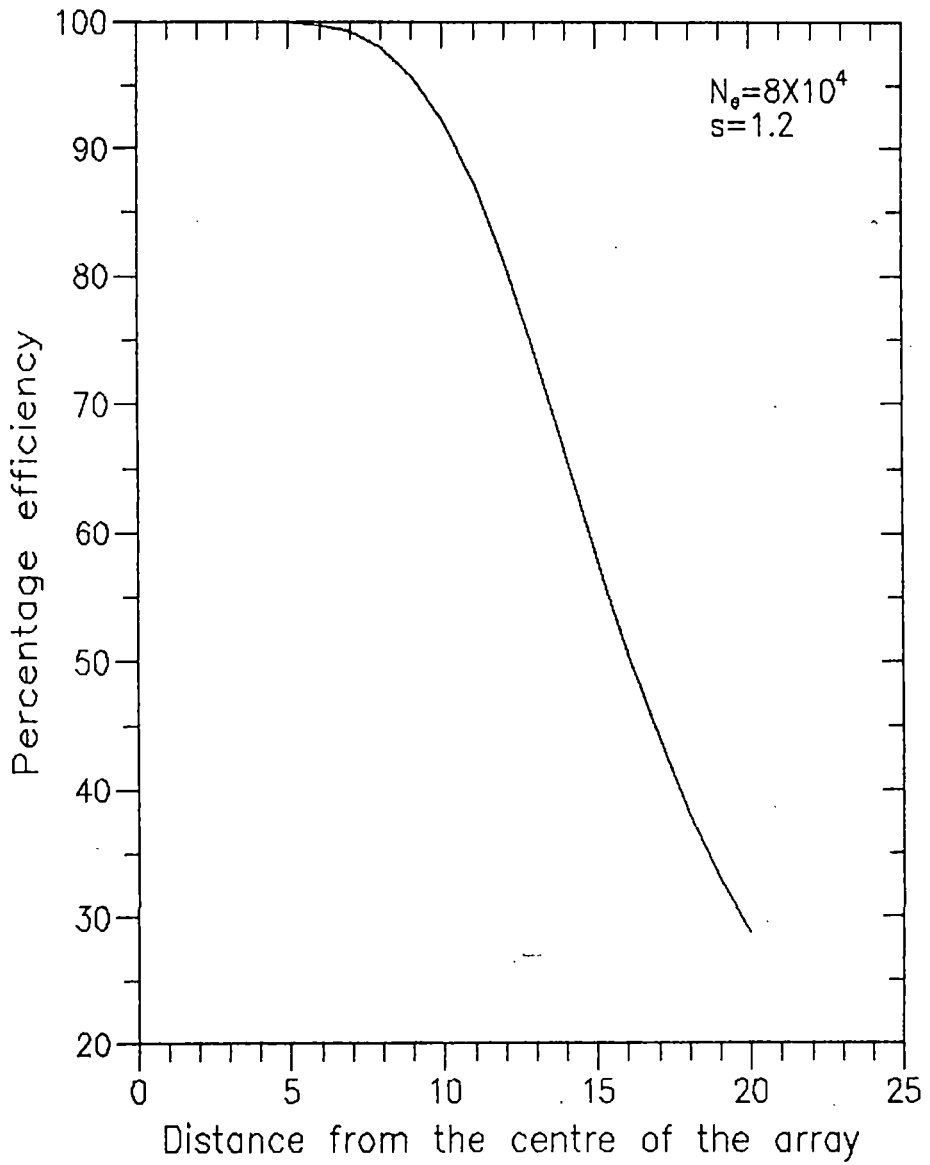


Fig.2.17. The detection efficiency of the array as a function of distance from the centre of the array for  $N_e = 8 \times 10^4$  and  $s = 1.2$

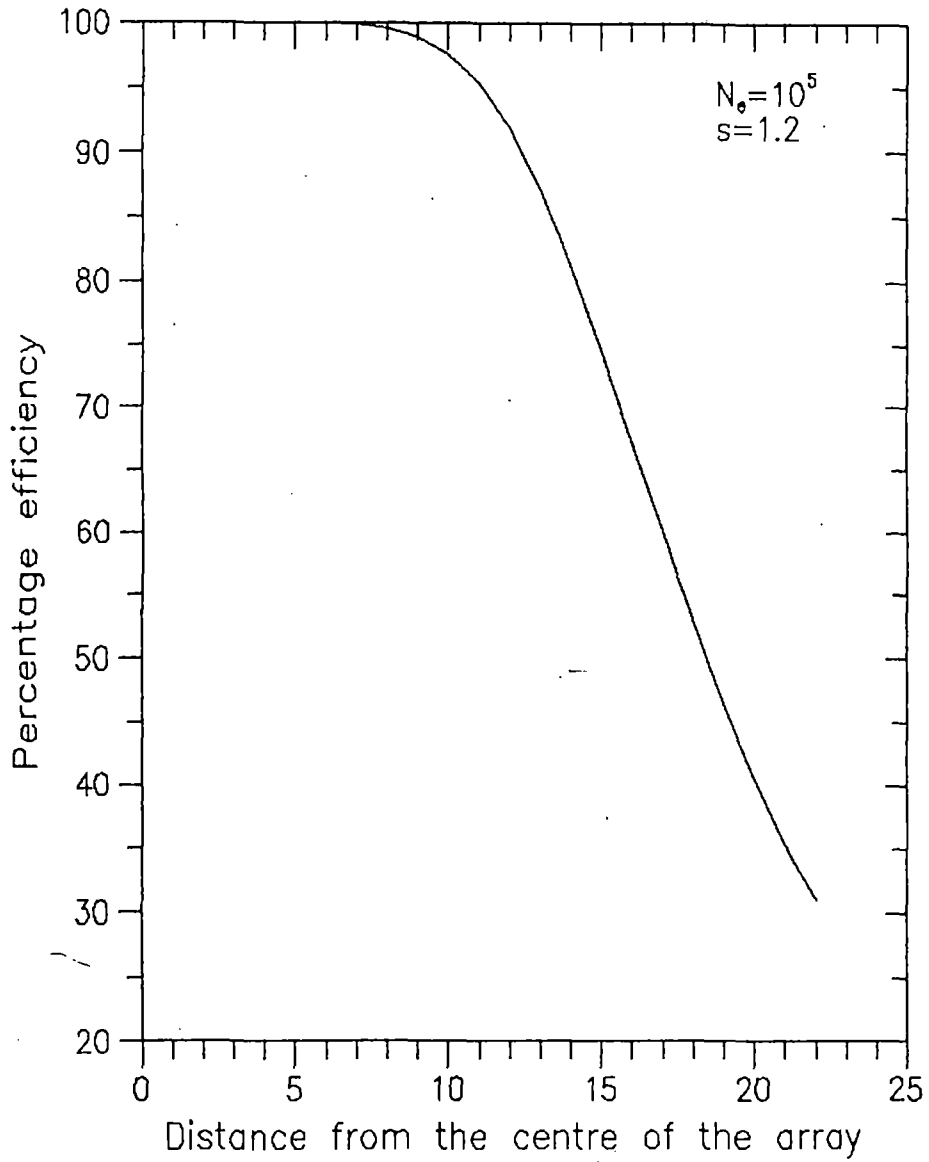


Fig.2.18. The detection efficiency of the array as a function of distance from the centre of the array for  $N_e=10^5$  and  $s=1.2$

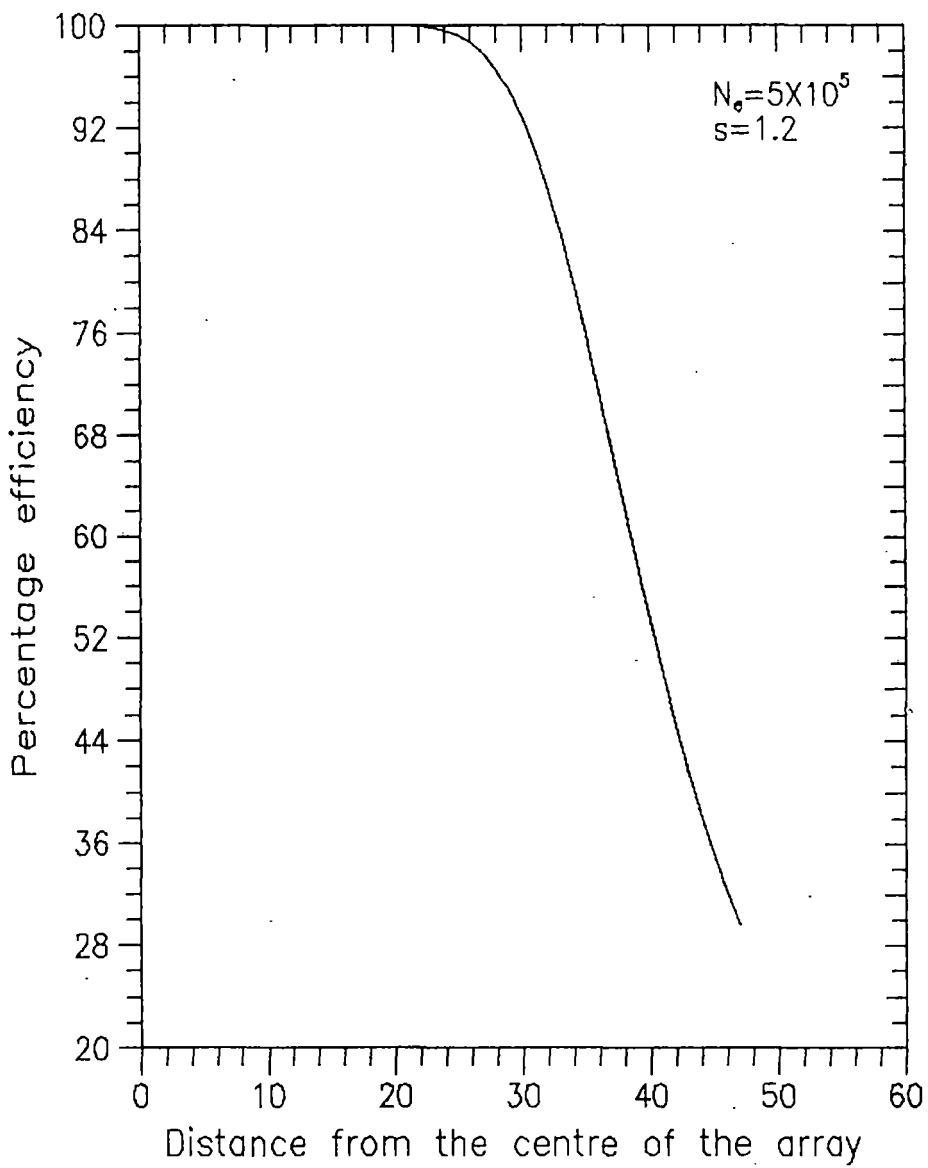


Fig.2.19. The detection efficiency of the array as a function of distance from the centre of the array for  $N_e = 5 \times 10^5$  and  $s = 1.2$



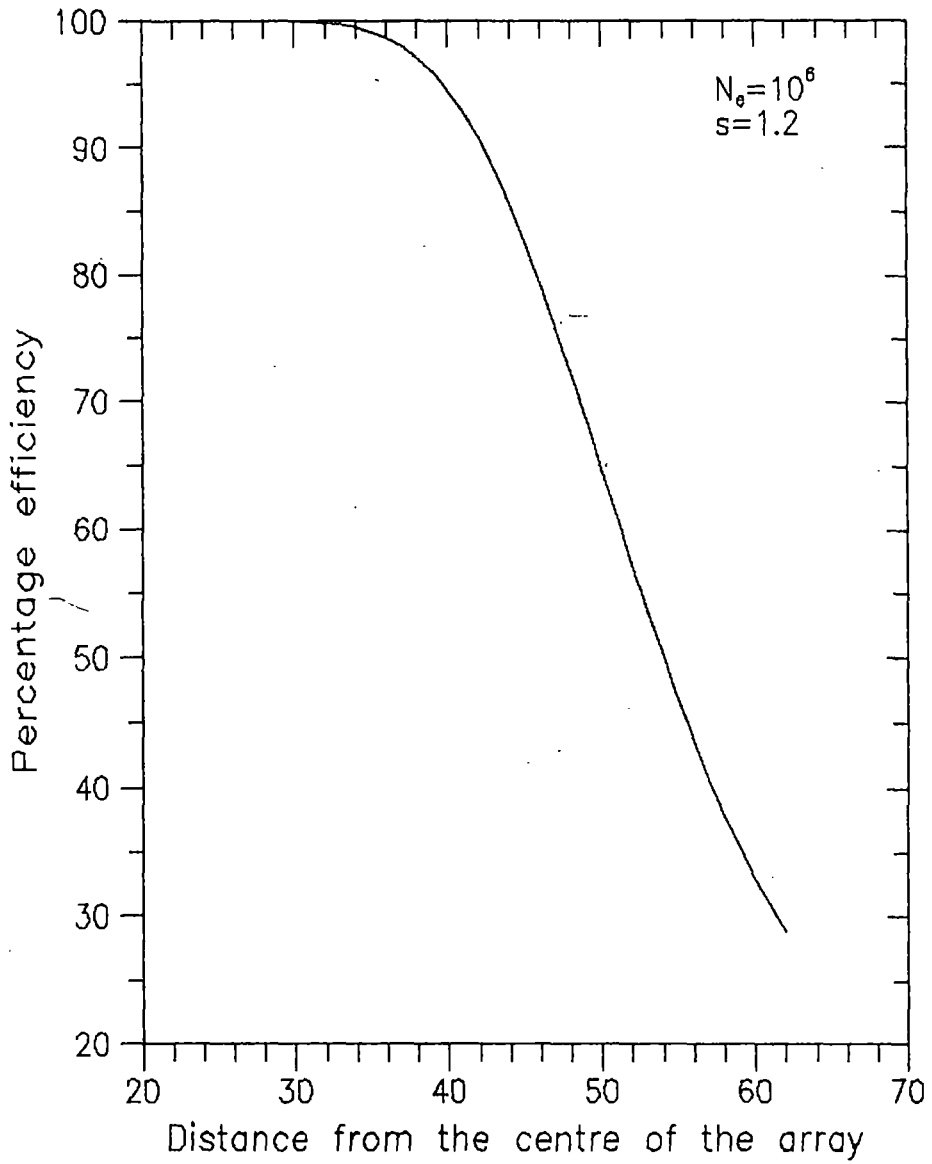


Fig.2.20. The detection efficiency of the array as a function of distance from the centre of the array for  $N_0=10^6$  and  $s=1.2$

### Triggering probability of the EAS array:

Calculation of the average triggering probability is based upon the assumption that the number of particles that are detected in a detector follow Poissonian statistics and if this is so then the triggering probability  $P_i$  is given by

$$P_i = \exp(-\Delta_i \cdot S_i) \sum_{n=m}^{\infty} (\Delta_i \cdot S_i)^n / n! \quad \text{-----}(2.11)$$

where  $\Delta_i$  is the particle density on the  $i$ th detector which is calculated by using Hillas function and  $S_i$  is the area of the  $i$ th detector whose particle threshold for detection is  $m$ .

The above relation is true only for detectors with no sampling errors, but in general the detectors have efficiencies that depend on both the number of particles incident on them and their particle threshold. If the efficiency is defined as  $\epsilon_i(n,m)$ , where  $n$  is the number of particles incident on the detectors and  $m$  is the particle threshold, then equation 2.11 becomes

$$P_i = \exp(-\Delta_i \cdot S_i) \sum_{n=0}^{\infty} [(\Delta_i \cdot S_i)^n / n!] \epsilon_i(n,m) \quad \text{-----} (2.12)$$

A useful modification to equation 2.12 is to write in such a way that it is not necessary to sum over an infinite number of particles but only  $k$  terms where  $k$  is the number of particles at which  $\epsilon_i$  becomes unity for the value of  $m$  in equation (2.12) and then

$$P_i = 1 - \exp(-\Delta_i \cdot S_i) \sum_{n=0}^k [ \{ (\Delta_i \cdot S_i)^n / n! \} \cdot \{ 1 - \epsilon_i(n,m) \} ] \quad \text{-----}(2.13)$$

Equation 2.13 is used to measure the average triggering probability of the EAS array as a function of shower size for different radial distances. The variation of average triggering probability with shower size for core-distances 20m, 30m and 40m from the centre of the array are shown in fig.2.21.

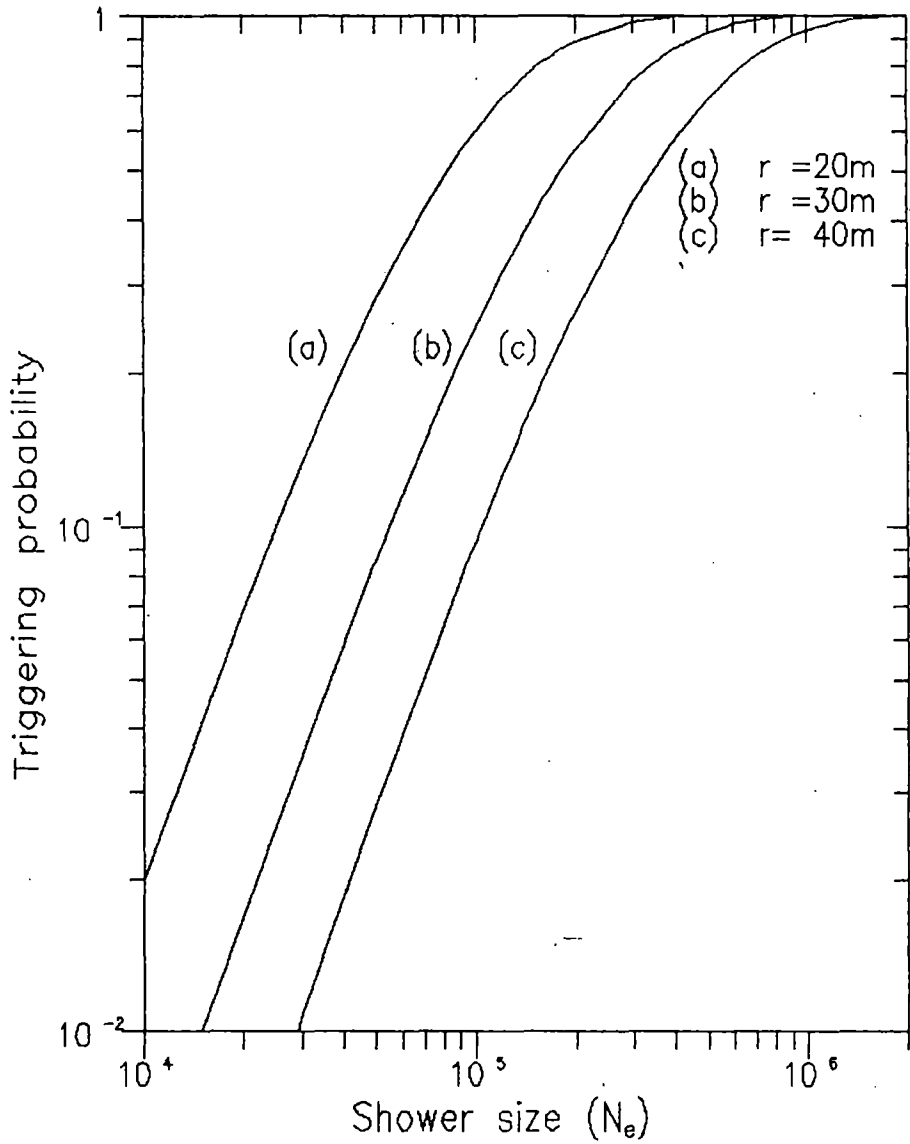


Fig.2.21. The average triggering probability for the array of detectors as a function of shower size for core distances 20m,30m and 40m